NACA RM E51F12

NACA

RESEARCH MEMORANDUM

TWO-DIMENSIONAL CASCADE INVESTIGATION OF THE MAXIMUM EXIT TANGENTIAL VELOCITY COMPONENT AND OTHER FLOW CONDITIONS AT THE EXIT OF SEVERAL TURBINE BLADE DESIGNS AT SUPERCRITICAL PRESSURE RATIOS

By Cavour H. Hauser and Henry W. Plohr

Lewis Flight Propulsion Laboratory
Cleveland, Ohio

NATIONAL ADVISORY COMMITTEE
FOR AERONAUTICS
WASHINGTON

August 23, 1951
Declassified June 26, 1956

NATIONAL ADVISORY COMMITTEE FOR AERONAUTICS

RESEARCH MEMORANDUM

TWO-DIMENSIONAL CASCADE INVESTIGATION OF THE MAXIMUM EXIT TANGENTIAL VELOCITY COMPONENT AND OTHER FLOW CONDITIONS AT THE EXIT OF SEVERAL TURBINE-BLADE DESIGNS AT SUPERCRITICAL PRESSURE RATIOS

By Cavour H. Hauser and Henry W. Plohr

SUMMARY

In order to evaluate the flow conditions within a gas turbine for the range of operating conditions near maximum turbine power output, an investigation of the flow through a two-dimensional cascade of turbine blades at supercritical pressure ratios was made. The nature of the flow at the exit of the blade row for the range of conditions represented by four different blade configurations was evaluated, thereby determining the range of application of a theoretical method for predicting the maximum exit tangential velocity component. The losses obtained in the two-dimensional cascade are presented in terms of a velocity coefficient. The effect of a reduction in the solidity from 2.16 to 1.68 was determined by comparing the results of two blade configurations having the same exit and entrance angles. Studies of the blade configurations having exit angles of 42.0°, 34.2°, and 20.0° measured from the tangential direction were compared to determine the effect of changing exit angle.

The experimental studies of the cascade included both static-pressure surveys and schlieren photographs. Pressure measurements were used to determine the velocities at the exit by the conservation-of-momentum principle.

The results of the investigation showed that, for the blades investigated, the general flow phenomena at the exit were essentially the same for all four blade configurations. Maximum turbine power output occurs when the shock wave that swings downstream along the suction surface finally reaches the blade trailing edge. When the pressure ratio is increased beyond this point, the losses become greater with no increase in turbine work.

The most significant change in performance caused by reducing the solidity from 2.16 for configuration I to 1.68 for configuration II was an increase in the velocity coefficient of as much as two points.

For blades of the type investigated, the maximum exit tangential-velocity component is a function of the blade geometry only and can be accurately predicted by the method of characteristics.

For a given angle of flow at the exit of the guided channel, a substantial increase in the maximum exit tangential velocity component can be obtained with curvature of the suction surface downstream of the exit of the guided channel.

For all four configurations, a maximum value of velocity coefficient is obtained at a pressure ratio immediately below that required for maximum blade loading followed by a sharp drop after maximum blade loading occurs.

INTRODUCTION

In the operation of axial-flow turbines for given inlet conditions and blade speed, a definite limitation occurs in the power output that can be obtained as the pressure ratio across the turbine is increased. In the design of an aircraft gas turbine, it is therefore necessary to predict the maximum power output to insure that the required turbine-power output for any condition of engine operation will fall within this limit. For fixed conditions at the turbine inlet, if the pressure ratio is increased beyond the point for which the blade passages are choked, thereby limiting the mass flow, the power output will continue to increase because of the supersonic expansion that occurs at the exit of a row of choked blade passages. Thus, in order to determine the nature of the flow within a turbine for operating conditions approaching maximum power output, an experimental study of the flow conditions at the exit of four turbine-blade configurations at supercritical pressure ratios has been made at the NACA Lewis laboratory with a two-dimensional cascade. The results of the investigation of the following problems associated with the condition of high turbine power output are presented herein:

(1) The nature of the flow within the blade passages for operational conditions in the range of maximum turbine power

(2) The blade design factors that affect the maximum power output

(3) The derivation of a theoretical method for the determination of the exit flow conditions and an experimental evaluation of the range of application

(4) An estimate of the losses associated with turbine operation at conditions in the range of maximum power

The four blade configurations studied were planned so that the effects of varying solidity and blade exit angle could be evaluated. The results obtained with configuration I, having a solidity based on axial width of 2.16 (2.32 based on blade chord), were compared with those of configuration II, having the same entrance and exit angles but a solidity of 1.68. The effect of changing blade-exit angle was determined by comparing the results obtained from configurations I, III, and IV having exit angles, measured from the tangential direction, of 34.2°, 42.0°, and 20.0°, respectively.

The results of a preliminary investigation of configuration I are presented in reference 1. The results presented herein were obtained when more extensive instrumentation was used.

In the experimental investigation of each of the blade configurations, a survey of the static-pressure distribution on the blade surface and downstream of the blade row was used to evaluate the velocity and the flow angle by the conservation-of-momentum principle. In addition, schlieren photographs of the flow through the passages were taken with the blades mounted between glass plates. All the experimental studies were carried out for an inlet temperature of 600° R, an inlet pressure within 5 percent of 22.0 pounds per square inch, and total-to-static pressure ratios from 1.89 to as high as 13.90.

SYMBOLS

The following symbols are used in this report:

A area, (sq ft)

K frictional drag force, (lb)

l flow path length along suction surface to center of area downstream of throat, (ft)

m mass flow, (slug/sec)

P pressure force, (lb)

p pressure, (lb/sq ft)

R_s Reynolds number, $\frac{l W_{av} \rho_{av}}{\mu_{av}}$

W relative velocity, (ft/sec)

β angle of flow measured from tangential direction, (deg)

δ angle of flow deviation, $\beta_3 - \beta_2$ (fig. 1), (deg)

γ ratio of specific heats, 1.40 for air

ρ mass density, (slug/cu ft)

μ absolute viscosity, (lb-sec/sq ft)

τ shearing stress due to boundary-layer friction, (lb/sq ft)

Subscripts:

a in the direction of blade suction surface at exit

av average on suction surface from leading edge to center of area downstream of throat used for computing Reynolds number

cr critical

n in the direction normal to blade suction surface at exit

s suction surface of blade downstream of throat

t trailing edge of blade

u tangential component

x axial projection or component

1 entrance to cascade

2 exit of cascade

3 station downstream of blade row where exit flow is evaluated

Superscript:

' stagnation state

THEORETICAL ANALYSIS

Method of Evaluation of Flow at Cascade Exit

The flow conditions downstream of the cascade were evaluated by the conservation-of-momentum principle as suggested in reference 2.

The equations of momentum conservation are applied to the mass of fluid enclosed by region ABCDEFGA shown in figure 1. When the components of momentum are resolved in directions parallel and perpendicular to the direction of flow at station 2, the velocity components at station 3, for the case of a straight suction surface downstream of and normal to the throat section, are

$$W_{a,3} = W_2 + \frac{P_2 - K_{a,s} - P_{a,3}}{m} \tag{1a}$$

$$W_{n,3} = \frac{P_{n,s} - P_{n,3}}{m} \tag{1b}$$

The pressure force P_2 acts in the direction of the velocity at this station and is composed of two parts: $\bar{p}_2 A_2$, the average pressure times the area at station 2 plus $\bar{p}_t A_t$, the pressure force over the trailing edge of the blade. The frictional drag $K_{a,s}$ is small compared with the pressure forces and therefore can be calculated with sufficient accuracy by assuming a turbulent boundary layer from the leading edge giving the equation (reference 3):

$$\frac{K_{a,s}}{A_s} = \bar{\tau}_s = \left[\frac{0.059}{(R_s)^{1/5}}\right]\left[\frac{\bar{\rho}_s(\bar{W}_s)^2}{2}\right] \tag{2}$$

The average values of density, velocity, and viscosity can be obtained from the static-pressure distribution on the blade surface assuming isentropic flow relations.

When the static pressure measured at station 2 is equal to the critical value, uniform sonic velocity can be assumed to exist at this station. The mass flow is calculated for this condition assuming isentropic flow upstream of this station and a flow coefficient of 1.

The pressure distribution over the surfaces A_s and $A_{x,3}$ are determined experimentally. The pressure forces acting on the jet boundaries CD and EF are equal and opposite and therefore have no effect on the flow. Frictional forces along these boundaries are neglected.

Maximum Obtainable Tangential Velocity for Given Blade-Exit Configuration

Because the pressure force P_3 has no component in the tangential direction, if the small frictional force $K_{a,s}$ is negligible, the tangential velocity component $W_{u,3}$ is dependent only on the momentum at station 2 and the pressure force P_s. The blade configuration shown in figure 2 has uniform sonic velocity across the throat section (station 2), which is parallel to the straight portion of the suction surface downstream of this station. For this configuration, the maximum possible tangential velocity at station 3 can be calculated by the method of characteristics and is a function only of the blade angle β_2. The tangential critical velocity ratio at the exit $(W_u/W_{cr})_3$ can be obtained from the momentum relation:

$$\left(\frac{W_u}{W_{cr}}\right)_3 = \left[\left(\frac{W}{W_{cr}}\right)_2 + \frac{P_2 - P_{n,s} \tan \beta_2}{m\, W_{cr}}\right] \cos \beta_2 \qquad (3)$$

Because the critical velocity ratio $(W/W_{cr})_2$ is equal to 1.0, the values of P_2 and m will be fixed for given inlet stagnation conditions. Apparently then, for these conditions, the exit tangential velocity component is dependent only on the blade angle β_2 and the pressure force $P_{n,s}$. The pressure distribution on the suction surface downstream of station 2 can be determined by the method of characteristics (reference 4) as shown in figure 2. When the pressure ratio is sufficient to cause the Prandtl-Meyer expansion around point B to extend along the suction surface to the trailing edge with a pressure distribution as shown in figure 2, the integral of the pressure distribution over the suction surface area downstream of the throat section $P_{n,s}$ will have reached a minimum value that will correspond to a maximum value of the tangential critical velocity ratio $(W_u/W_{cr})_3$. As the angle β_2 is decreased, this minimum value of $P_{n,s}$ obtained for maximum blade loading is lowered, giving even higher possible tangential velocities than would be expected from the changes in the values of $\tan \beta_2$ and $\cos \beta_2$ alone. The analysis by the method of characteristics for $\gamma = 1.40$ was made over a range of values of exit angle for the blade configuration shown in figure 2; the results are plotted in figure 3 which gives the maximum attainable exit tangential velocity component as a function of the angle β_2. The experimental verification of this curve is discussed later in the report.

EXPERIMENTAL APPARATUS AND PROCEDURE

Blade Design

The four blade configurations that were experimentally investigated in the cascade are shown in figure 4. Two different blade profiles were used to make up the four configurations. The channel between blades was designed on the basis of one-dimensional-flow theory in order that the velocity would continually increase to the throat section (station 2). Configuration I (fig. 4(a)) is made up of high-reaction blade profiles (blade 1) having a blade exit angle β_2 of 34.2° and a solidity of 2.16 based on the axial width.

In order to determine the effect of lowered blade solidity on the exit flow conditions, the blades used in configuration I were spaced further apart and the blade angles β_1 and β_2 were held constant in configuration II (fig. 4(b)). The solidity for this configuration was 1.68.

Configurations III and IV were investigated and compared with I to determine the effect of changing the blade exit angle β_2 on the exit flow conditions. Configuration III (fig. 4(c)) is made up of low-reaction blade profiles (blade 2) having an exit angle β_2 of 42.0° and a solidity of 2.16. Configuration IV (fig. 4(d)) is made using blade 1 with the angle of the profiles changed to give very high reaction and a blade exit angle of 20°. The solidity is 1.41. This configuration is representative of a turbine-stator design.

For configurations I, II, and III, the portion of the suction surface downstream of the guided channel is a straight line parallel to the direction of flow at the throat section. For configuration IV, the straight portion of the suction surface downstream of the guided channel makes an angle of 20.0° with respect to the tangential direction while the flow direction at the throat is at an angle of 31.0°. This latter configuration requires the attached flow on the suction surface to turn an additional 11° downstream of the throat section.

Experimental Equipment

Two experimental test sections were made up for each of the four configurations, one for making static-pressure surveys and another for obtaining schlieren photographs. The axial width of the blades was 1.80 inches for configurations I, II, and III and 1.58 inches for configuration IV. The blade height was 2.00 inches for all four configurations.

The static-pressure survey test section of configuration I is shown in figure 5. The cascade of six blades and two end blocks,

forming seven equal passages, was mounted between two static-pressure tapped steel plates. Measurements obtained from the 13 static-pressure taps 0.39 inch upstream of the blades were used in order to determine the uniformity of the flow at the entrance to the cascade. Static-pressure measurements obtained from the 21 taps upstream of the throat section on the pressure and suction surfaces of the center passage were used to show that the velocity in the channel approached sonic speed. These measurements were also used to obtain average values of velocity and density used in the calculation of the Reynolds number R_s. A total of 11 static-pressure taps, spaced approximately 1/16 inch apart on the straight portion of the suction surface downstream of the throat, were used to obtain the pressure distribution over the area A_s. The pressure distribution at station 3 was obtained from 33 static-pressure taps 0.39 inch downstream of the blade row. The static-pressure-survey test sections of configurations II, III, and IV had similar instrumentation. The cascade of configuration III also had seven equal passages and configurations II and IV had five equal passages.

Schlieren photographs of the flow through each cascade configuration were obtained from a test section with optical glass plates substituted for the steel plates used in the pressure-survey tests. The blades were pinned to four steel bars about 0.10 inch square in cross section that were inlaid in slots ground in the glass plates. Static-pressure taps in the exhaust ducting were observed for both the static-pressure surveys and the optical tests in order to correlate the schlieren photographs with pressure-survey data.

For all cascade tests, air from the high-pressure air-supply system of the laboratory was passed through a steam-supplied heat exchanger to a surge tank, 42 inches in diameter and 72 inches in length, at the entrance of the test section. The heat exchanger was used to raise the inlet-air temperature to 600° R in order to avoid the possibility of encountering condensation shocks in the test section. The surge tank contained a diaphragm of fine-mesh screens and a bank of flow-straightening tubes for equalizing the velocity distribution over the area of the tank. The test section was mounted directly on the downstream end plate of the surge tank (fig. 6). Air from the test section was exhausted to the low-pressure exhaust system of the laboratory. Two large horizontal wooden nozzle blocks guided the air from the inside of the surge tank into the test section. Provision was made for drawing off the boundary-layer air from the horizontal walls $1\frac{3}{8}$ inches upstream of the cascade. The boundary-layer slots extended over the width of the cascade and were divided into four equal sections each having an individual valve for metering the flow. The air from these boundary-layer ducts was exhausted to the low-pressure system of the laboratory.

The inlet total pressure and temperature were measured in the surge tank just upstream of the cascade. The inlet total temperature was measured with a thermocouple and read on a potentiometer to within 1° F. The static pressures were read on manometers to an accuracy within 0.05 pound per square inch. All the experimental studies were carried out for an inlet temperature of 600° R, an inlet pressure within 5 percent of 22.0 pounds per square inch, and total-to-static pressure ratios from 1.89 to as high as 13.90.

Calculation Methods for Static-Pressure-Survey Data

The exit flow conditions were evaluated by the conservation-of-momentum principle (equation (1)) using the experimental data obtained from the static-pressure surveys. The flow was assumed to be isentropic from the stagnation conditions in the surge tank to critical conditions at the blade throat section. The mass flow was calculated for these assumed conditions at station 2 and an assumed flow coefficient of unity.

For configurations I, II, and III, the pressure force $P_{n,s}$ was evaluated by integrating a plot of the static-pressure distribution over the area A_s. The pressure $\bar{p}_t$ was read from these plots at the point corresponding to the trailing-edge point F. The frictional drag force $K_{a,s}$ was evaluated by equation (2) using average values of density and velocity obtained from the static-pressure distribution assuming isentropic-flow conditions. The pressure force P_3 was obtained from an integration of the pressure distribution along the survey line at station 3.

Evaluation of the exit flow conditions for configuration IV were made in a similar manner, when equation (1) was used in a modified form. This modification was necessary in order to account for the 11° of turning downstream of station 2.

A velocity coefficient, defined as the ratio of the calculated velocity at station 3 to the isentropic velocity corresponding to the static pressure at that station, was evaluated. The efficiency of the expansion through the blade row is equal to the square of this velocity coefficient.

RESULTS AND DISCUSSION

The results of the analyses based on the static-pressure surveys are shown in figure 7. The flow deviation angle, the velocity components at the exit of the blade row, and the velocity coefficient are plotted against the total-to-static pressure ratio p'_1/p_3. Schlieren

photographs of the flow past each blade configuration at various pressure ratios are shown in figures 8 to 11. The pressure ratios for which the various schlieren photographs were taken are indicated in figure 7.

Exit Flow Conditions Obtained with Increasing Pressure Ratio

The general flow phenomena downstream of the guided channel of the blade were the same for all four configurations. The results obtained for configuration I shown in figure 7(a) are typical. As the pressure ratio p'_1/p_3 is increased beyond the value required to obtain sonic velocity at the throat section at the exit of the guided channel, the flow immediately downstream of this station becomes supersonic, followed by an oblique shock wave, as shown in figure 8(a). Further increases in the pressure ratio cause the supersonic region upstream of the shock wave to be extended and the angle of the shock wave becomes more acute (fig. 8(b)). A second shock wave is seen to originate from the flow separating from the suction surface side of the trailing edge. The velocity at station 3 shown in figure 7(a) continues to increase at a fairly constant angle until a pressure ratio of 2.75 is attained. At this point the trailing-edge portion of the blade is fully loaded; that is, the velocities on the suction surface have attained maximum values, and the exit tangential critical velocity ratio remains constant at a value of 1.0. Maximum blade loading occurs when the oblique shock wave that swings downstream along the blade suction surface finally reaches the blade trailing edge. This condition is shown in figure 8(c). The experimental velocity distribution over the trailing-edge portion of the blade suction surface for this condition is the same as that calculated by the method of characteristics, as shown in figure 2. The maximum tangential component $(W_u/W_{cr})_3$ of 1.0 is apparently in close agreement with the theoretical value at the blade angle β_2 of 34.2° in figure 3. It would be undesirable to use pressure ratios greater than that required for maximum blade loading in an actual turbine. Greater losses would be encountered in the exit shock wave pattern as shown in figures 8(d) and 8(e) without an increase in the work output of the turbine. In analyzing the velocity coefficients, it is important to note that the values plotted in figure 5 are an indication of the losses upstream of survey station 3 only; for example, for configuration I, the velocity coefficient is a maximum at pressure ratios immediately below that required for maximum blade loading. The coefficient drops off sharply after maximum blade loading is obtained and increases slightly at pressure ratios greater than 3.40. This rise in the measured velocity coefficient occurs when the shock waves, which originate from the separation of the flow from the pressure surface, move downstream of the survey station so that the losses occurring in these shock waves do not affect the measured velocity coefficient. The shock wave patterns in figures 8(d) and 8(e) show the manner in which this occurs.

Effect of Solidity

A comparison of the results presented in figures 7(a) and 7(b) indicates that the main effect of the change in solidity from 2.16 for configuration I to the value of 1.68 for configuration II is to raise the velocity coefficient as much as two points. Evidently the improvement in efficiency is caused by the reduced wake losses that are due to the reduction in the number of blades.

The velocity components for configurations I and II show approximately the same pattern. The tangential velocity component $(W_u/W_{cr})_3$ is slightly higher over the whole range of pressure ratios for configuration II but reaches a maximum value for both configurations at a pressure ratio of about 2.75.

The deviation angle for configuration II is somewhat lower than that of configuration I for the low pressure ratios; however, the deviation angles are approximately equal for both configurations at pressure ratios greater than 2.75 where maximum blade loading is obtained. Apparently the angle of flow and the velocity coefficient are rather erratic and unpredictable until maximum blade loading is approached because of the interaction of shock wave and boundary layer along the trailing-edge portion of the suction surface. A comparison of the schlieren photographs in figures 8 and 9 indicates that differences in flow angle of about 3° or 4° might be caused by the different shock-wave patterns at the blade exit. As the discussion in reference 5 indicates, the flow conditions at the trailing edge of an airfoil are dependent on the Reynolds number and the boundary-layer thickness just upstream of the point of separation, and therefore prediction of the conditions in this region is difficult. After maximum blade loading is obtained, however, conditions upstream of the blade trailing edge become stabilized. The deviation angle then increases constantly with increasing pressure ratio as the axial component increases with constant tangential velocity.

Effect of Blade Exit Angle

A comparison of the results in figures 7(a), 7(c), and 7(d) shows the change in blade performance that results from the variation in blade exit angle for configurations I, III, and IV, respectively. The pressure ratio corresponding to maximum blade loading increases markedly as the blade angle is decreased. Thus for configuration III, for which the exit angle is 42.0°, maximum blade loading is obtained at a pressure ratio of 2.3, whereas for configuration IV, with an exit angle of 20.0°, maximum loading is not obtained until the pressure ratio is about 3.5.

The experimental value of the maximum tangential velocity component $(W_u/W_{cr})_3$ is in excellent agreement with the theoretical value for all

four configurations. The experimental values obtained for configurations I, II, and III are plotted in figure 3. For configuration IV, the curvature of the suction surface continues downstream of the exit of the guided channel; therefore, a separate analysis by the method of characteristics was made for this configuration in a manner similar to that shown in figure 2. The maximum value of $(W_u/W_{cr})_3$ obtained theoretically in this manner was 1.17, which is in satisfactory agreement with the maximum experimental value of 1.18. Because the passage is choked at the exit of the guided channel, the mass flow will be determined by the angle of flow at this station and the trailing-edge thickness of the blade. The 11° of turning along the suction surface downstream of this station was therefore effective in providing a substantial increase in the exit tangential velocity $(W_u/W_{cr})_3$ from the value of 1.08 corresponding to a blade angle β_2 of 31° (fig. 3) without decreasing the mass flow.

Apparently for configurations III and IV, as well as I and II, the angle of flow is rather erratic until the blade is fully loaded. For configuration IV, especially, the deviation angle varies as much as 9° for small changes in pressure ratio. Evidently greater flow instability exists at the high Mach numbers along the suction surface near the trailing edge of the blades in configuration IV. The deviation angle is positive over the whole range of pressure ratios for configuration IV. At the low pressure ratios, the positive deviation angle is caused by a tendency for the flow to separate a varying degree from the suction surface near the trailing edge which is turned 11° tangentially from the flow direction at the exit of the guided channel. After the blade is fully loaded, the deviation angle remains positive because of the acceleration of the axial velocity component at station 3 while the tangential component remains constant.

In order to estimate the magnitude of the losses occurring in the shock waves downstream of survey station 3, a theoretical analysis by the method of characteristics was made for configuration I at a pressure ratio of about 3. At this pressure ratio, maximum blade loading is obtained and the shock-wave pattern can be simplified as two single oblique shock waves originating from the separation of the flow from either side of the blade trailing edge. The shock-wave positions were measured from the schlieren photograph of figure 8(c). The total-pressure loss experienced by the flow from one passage crossing successive shock waves was evaluated until the shock strength was negligible. The theoretical velocity coefficient obtained from this analysis, that considers the shock losses only, is 0.991 at station 3, whereas further downstream, where the shock losses have become negligible, the velocity coefficient is 0.978. The measured value at station 3 (fig. 7(a)) is 0.958 for this condition. The additional losses measured experimentally are probably due to viscous effects. Even though the theoretical shock losses downstream of station 3 are greater than those upstream of this

station, the over-all loss due to the shock waves is not large. The theoretical velocity coefficient of 0.978 corresponds to an efficiency of 0.957. The experimental results indicate that some improvement in efficiency may be realized by operating the blade at a pressure ratio just below the ratio required for maximum blade loading. Figure 7(a) indicates that at a pressure ratio of about 2.6 the experimental velocity coefficient is 0.976, whereas the tangential velocity component is negligibly smaller than the maximum values at this pressure ratio. The improved efficiency is evidently caused primarily by decreased shock-wave strength at the lower pressure ratio.

The velocity coefficient for configurations III and IV shows the same general pattern as those of configurations I and II. A maximum value of velocity coefficient is obtained at a pressure ratio immediately below that required for maximum blade loading followed by a sharp drop after maximum blade loading occurs. As before, the gradual rise in velocity coefficient at the higher pressure ratios is caused by the movement of the trailing-edge shock waves downstream of survey station 3. A comparison of the velocity coefficient for configuration IV with those of reference 6 shows that even though different methods of evaluation were used, the velocity coefficients obtained are of the same order of magnitude.

SUMMARY OF RESULTS

An experimental study of the flow conditions at the exit of four turbine-blade configurations at supercritical pressure ratios has been made in a two-dimensional cascade. The following results were obtained:

1. For the blades investigated having uniform sonic velocity at the exit of the guided channel and nearly straight suction surface downstream of this station, the general flow phenomena downstream of the guided channel at supercritical pressure ratios were essentially the same for all four configurations. The maximum blade loading, corresponding to maximum turbine power, is obtained when the shock wave which swings downstream along the suction surface finally reaches the blade trailing edge. Increasing the pressure ratio beyond this point increases the losses with no increase in turbine work.

2. The most significant change in performance caused by reducing the solidity from 2.16 for configuration I to 1.68 for configuration II was to increase the velocity coefficient as much as two points.

3. For blades of the type investigated, the maximum exit tangential velocity component is a function of the blade geometry only and can be accurately predicted by the method of characteristics.

4. For a given angle of flow at the exit of the guided channel where the passage is choked, thereby limiting the turbine mass flow, a substantial increase in the maximum exit tangential velocity component can be obtained with curvature of the suction surface downstream of the exit of the guided channel.

5. For all four configurations, a maximum value of velocity coefficient is obtained at a pressure ratio immediately below that required for maximum blade loading followed by a sharp drop after maximum blade loading occurs.

Lewis Flight Propulsion Laboratory,
National Advisory Committee for Aeronautics,
Cleveland, Ohio, May 17, 1951.

REFERENCES

1. Hauser, Cavour H., Plohr, Henry W., and Sonder, Gerhard: Study of Flow Conditions and Deflection Angle at Exit of Two-Dimensional Cascade of Turbine Rotor Blades at Critical and Supercritical Pressure Ratios. NACA RM E9K25, 1950.

2. Stodola, A.: Steam and Gas Turbines. Vol. I. McGraw-Hill Book Co., Inc., 1927, pp. 136-146.

3. Rouse, Hunter: Fluid Mechanics for Hydraulic Engineers. McGraw-Hill Book Co., Inc., 1938, pp. 203-204.

4. Liepmann, Hans Wolfgang, and Puckett, Allen E.: Introduction to Aerodynamics of a Compressible Fluid. John Wiley & Sons Inc., 1947, pp. 189-232.

5. Chapman, Dean R.: An Analysis of Base Pressure at Supersonic Velocities and Comparison With Experiment. NACA TN 2137, 1950.

6. Kraft, Hans: Reaction Tests of Turbine Nozzles for Subsonic Velocities. A.S.M.E. Trans., vol. 71, no. 7, Oct. 1949, pp. 781-787.

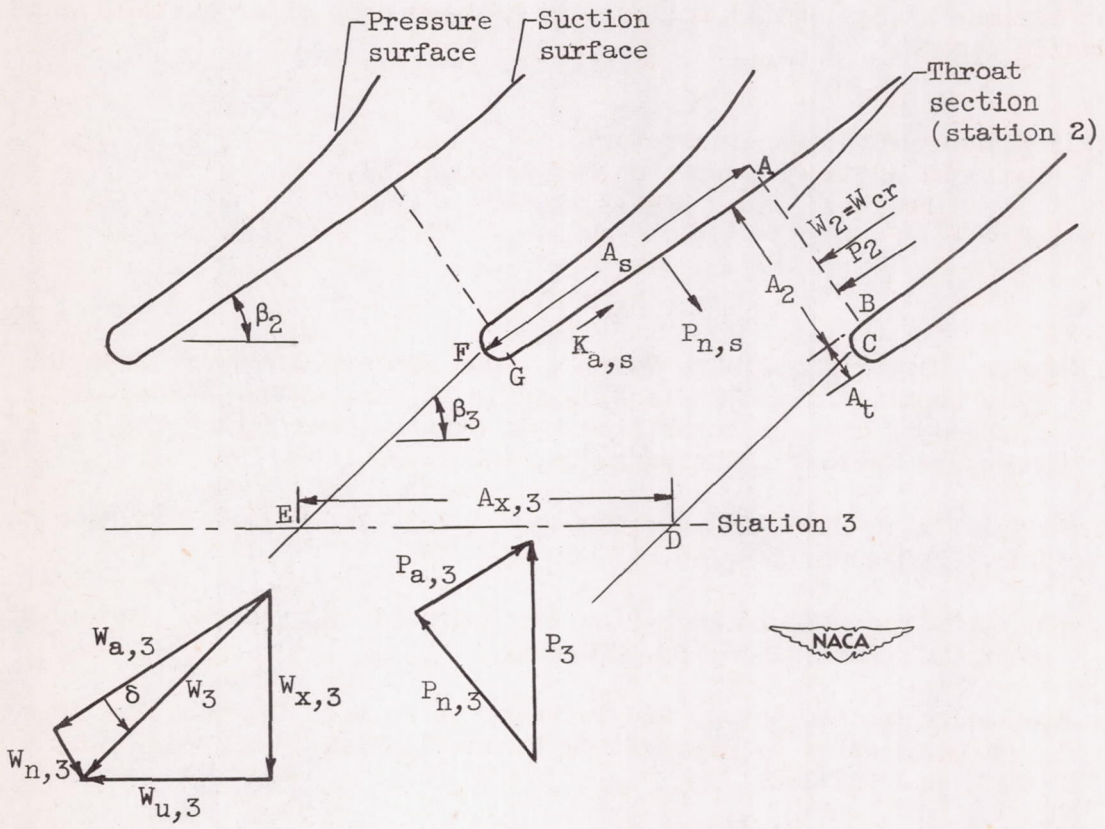

Figure 1. - Diagram of flow conditions at exit of cascade of turbine rotor blades at supercritical pressure ratios for analysis using conservation-of-momentum principle and measured values of static-pressure distribution.

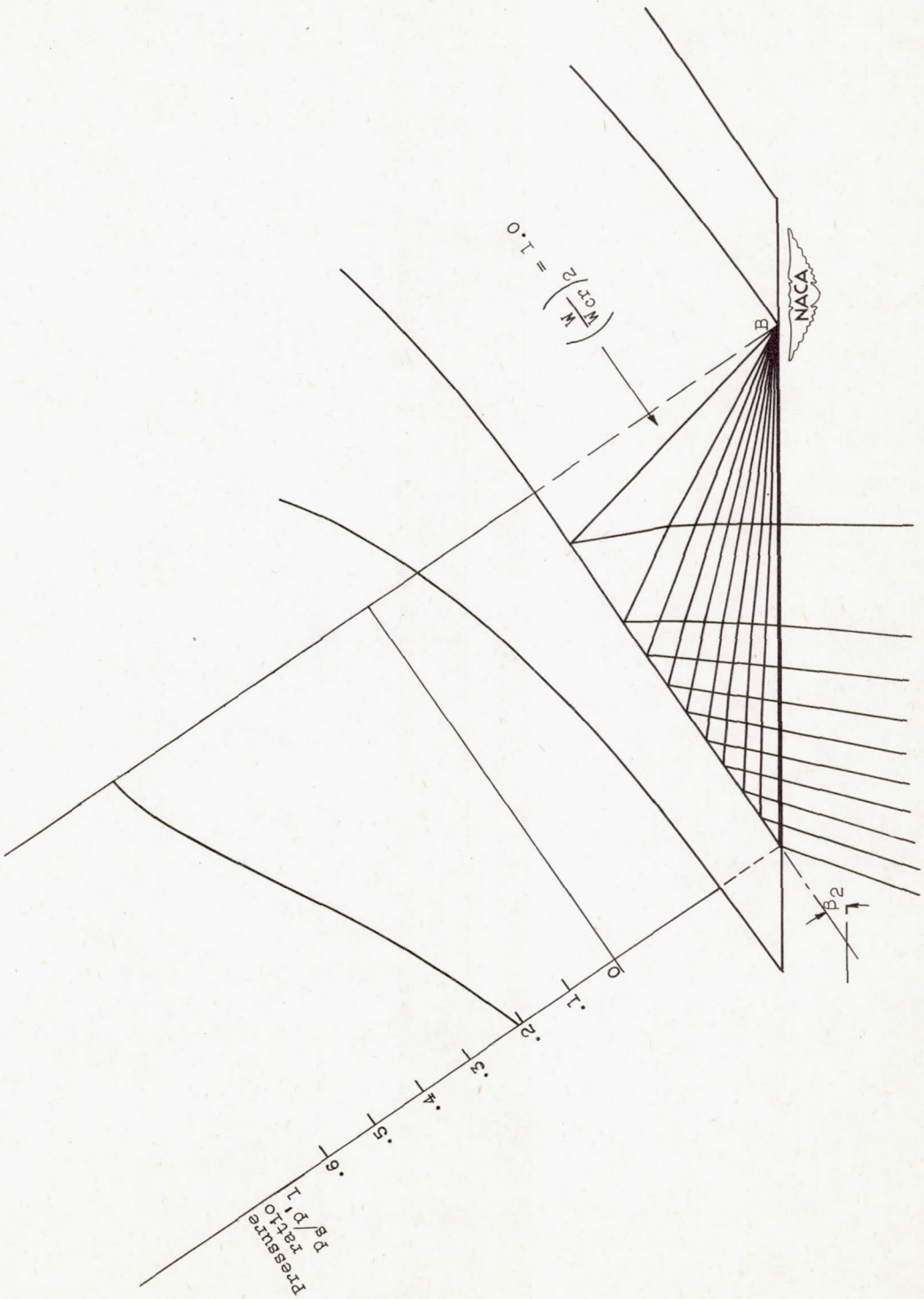

Figure 2. - Characteristic diagram and static-pressure distribution on downstream portion of blade profile for maximum blade loading.

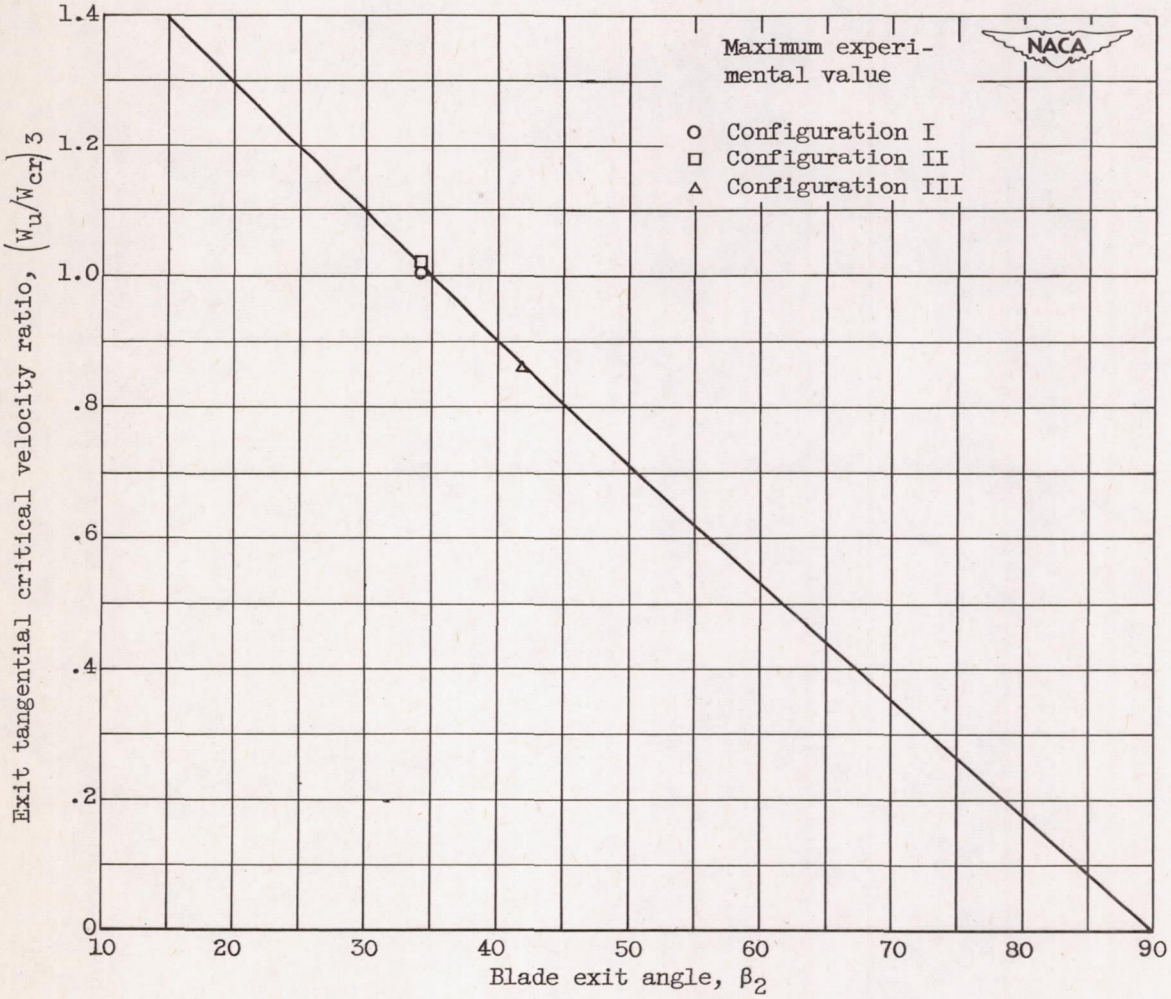

Figure 3. - Maximum tangential velocity component determined by method of characteristics for turbine blade with fully loaded, straight suction surface downstream of and normal to throat section at exit of guided channel.

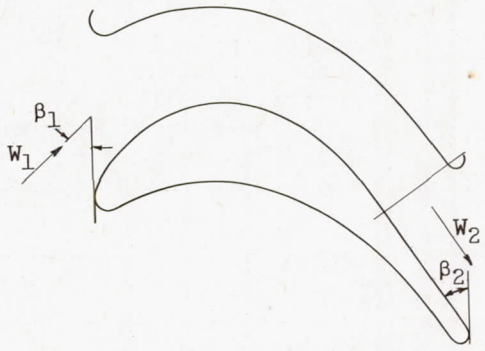

(a) Blade configuration I. Blade 1: β_1, 48.5°; β_2, 34.2°; solidity, 2.16.

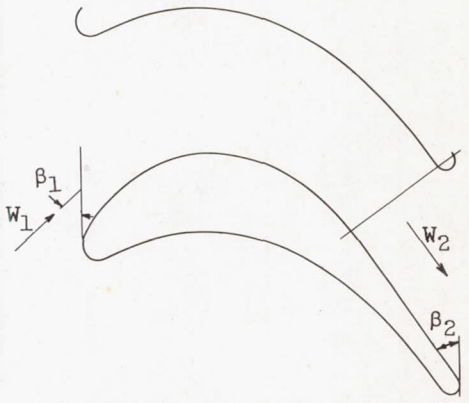

(b) Blade configuration II. Blade 1: β_1, 48.5°; β_2, 34.2°; solidity, 1.68.

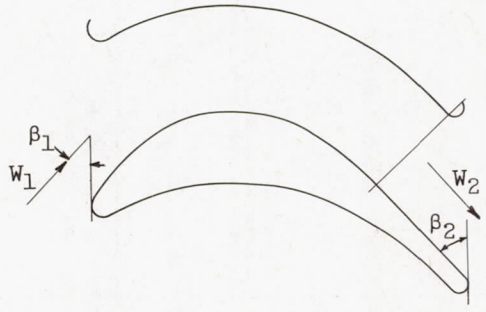

(c) Blade configuration III. Blade 2: β_1, 45.0°; β_2, 42.0°; solidity, 2.16.

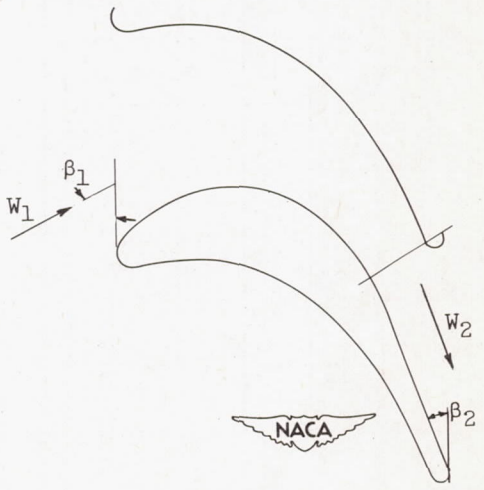

(d) Blade configuration IV. Blade 1: β_1, 62.6°; β_2, 20.0°; solidity, 1.41.

Figure 4. - Blade configurations studied.

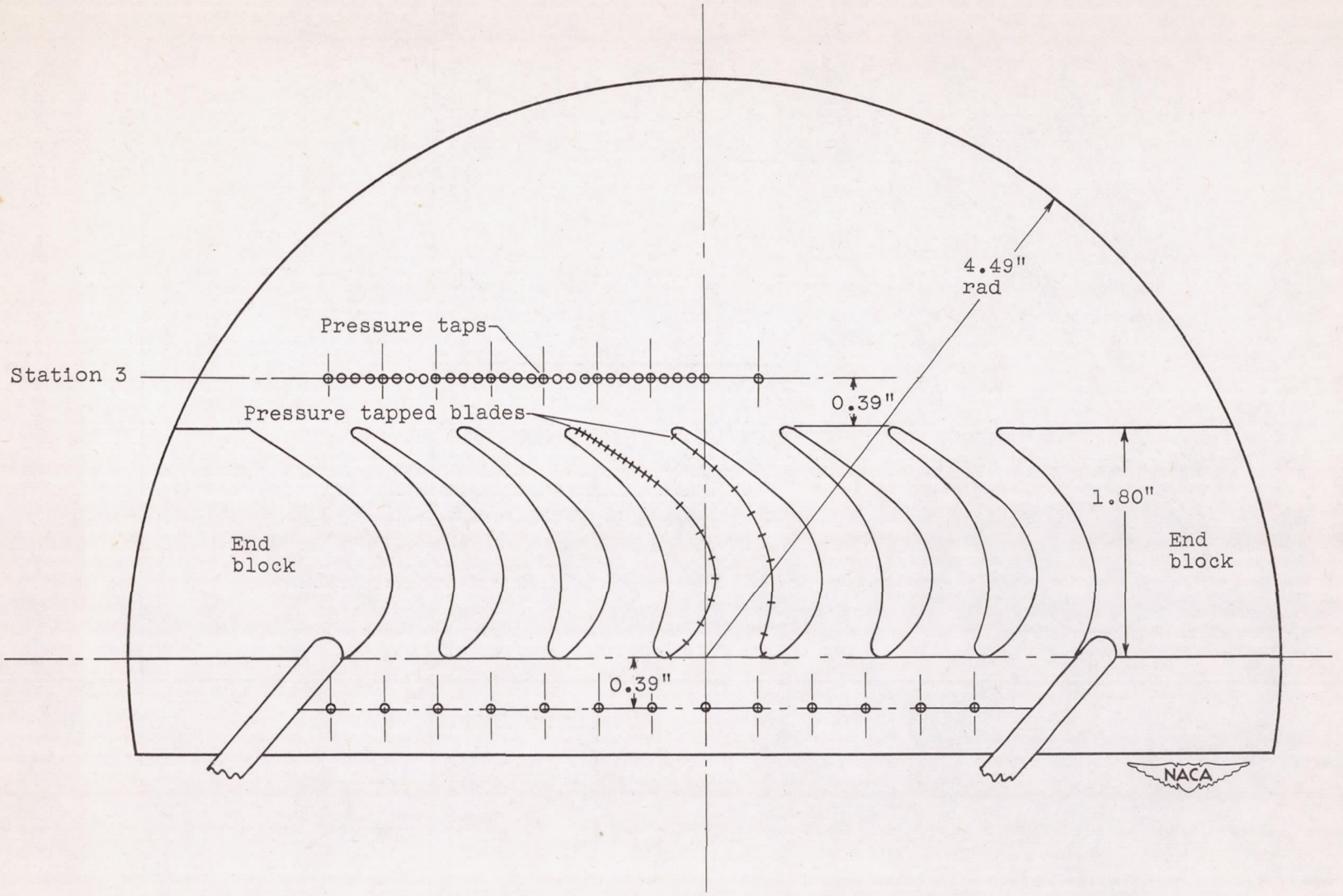

Figure 5. - Plan view of static-pressure-survey test section with blade configuration I installed.

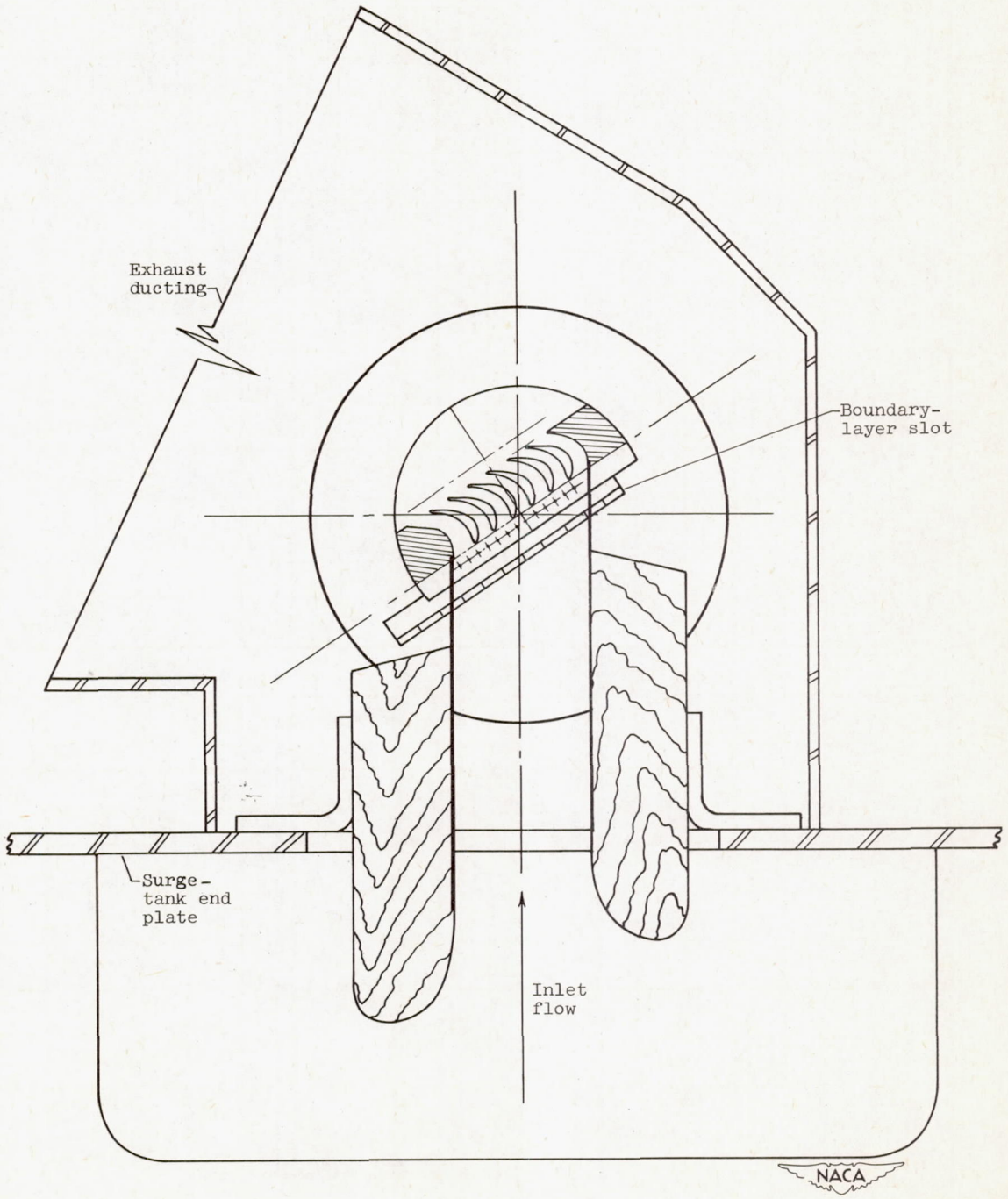

Figure 6. - Plan view of cross section through over-all test section assembly.

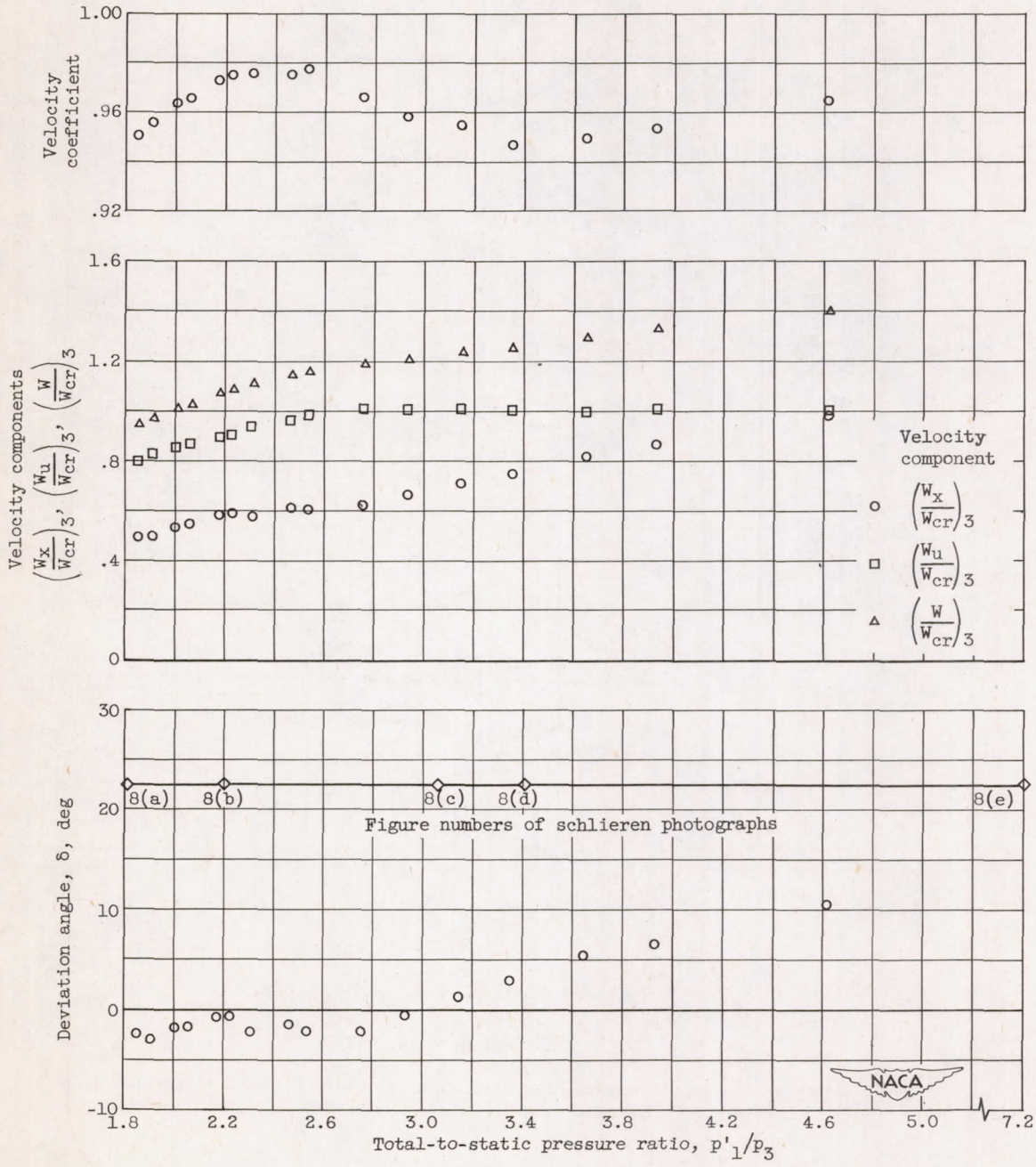

(a) Configuration I.

Figure 7. - Flow conditions at exit of cascade (station 3) determined from static-pressure surveys.

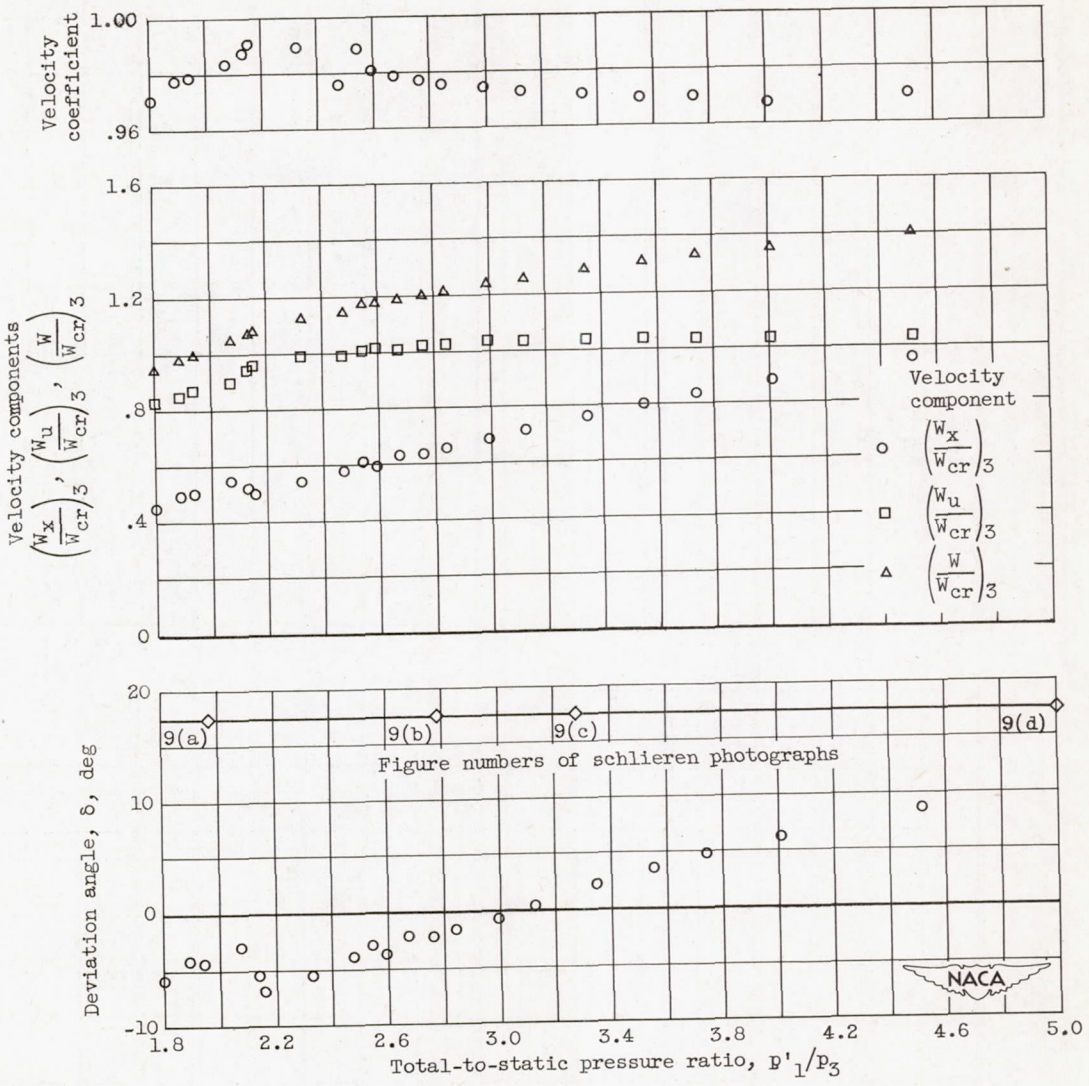

(b) Configuration II.

Figure 7. - Continued. Flow conditions at exit of cascade (station 3) determined from static-pressure surveys.

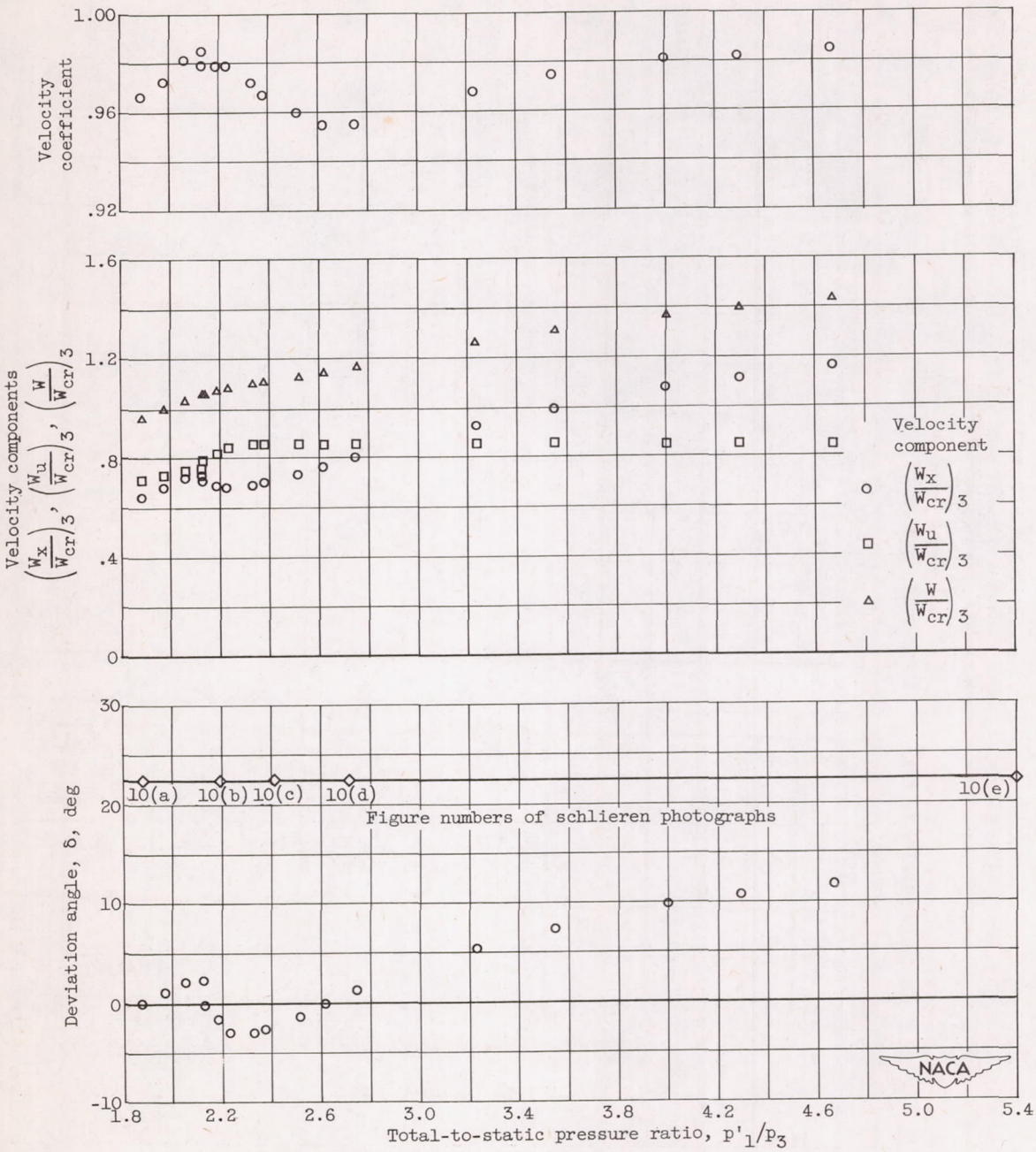

(c) Configuration III.

Figure 7. - Continued. Flow conditions at exit of cascade (station 3) determined from static-pressure surveys.

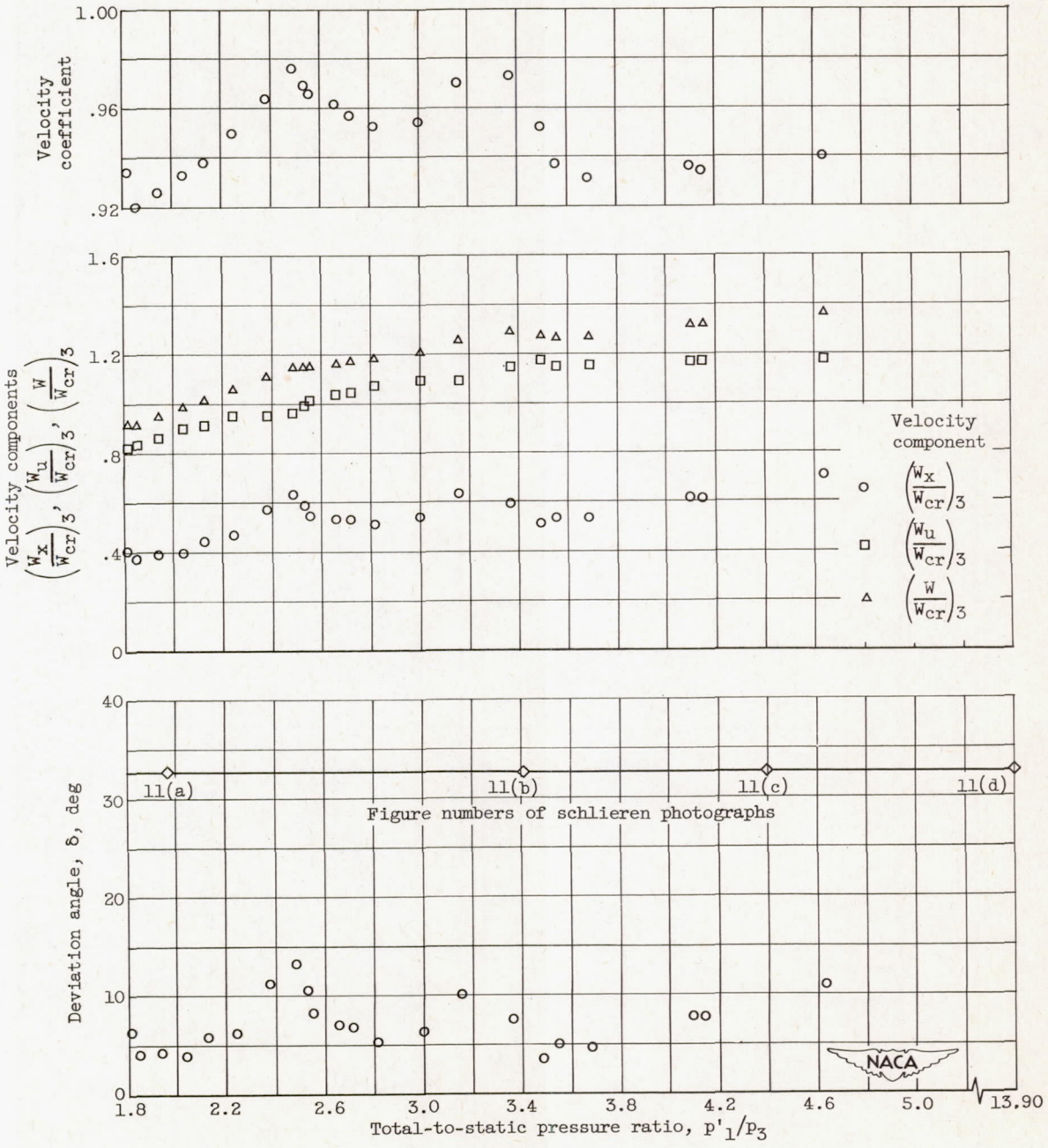

(d) Configuration IV.

Figure 7. - Concluded. Flow conditions at exit of cascade (station 3) determined from static-pressure surveys.

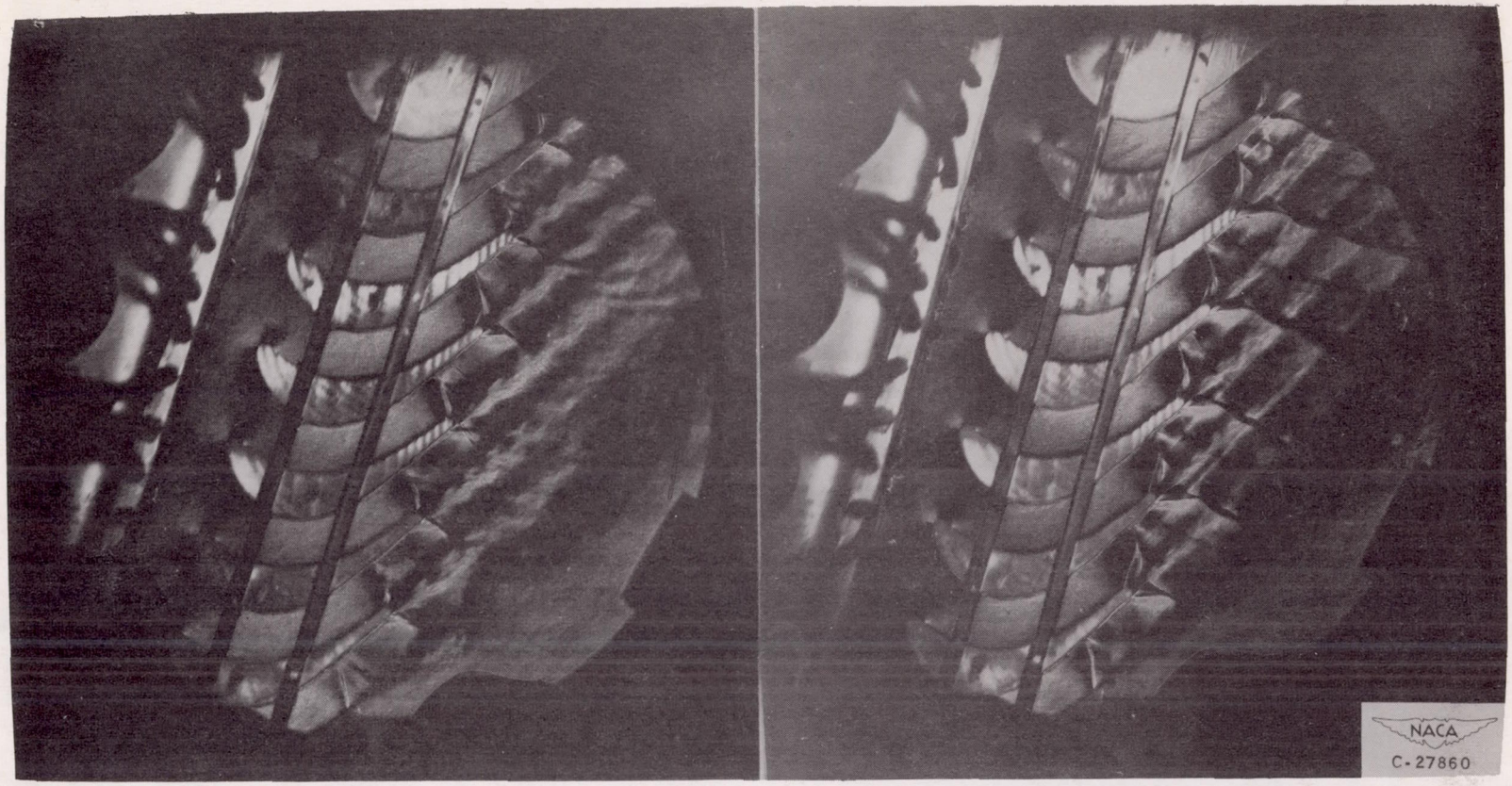

(a) Schlieren photograph; total-to-static pressure ratio, 1.82.

(b) Schlieren photograph; total-to-static pressure ratio, 2.20.

Figure 8. - Optical studies of configuration I.

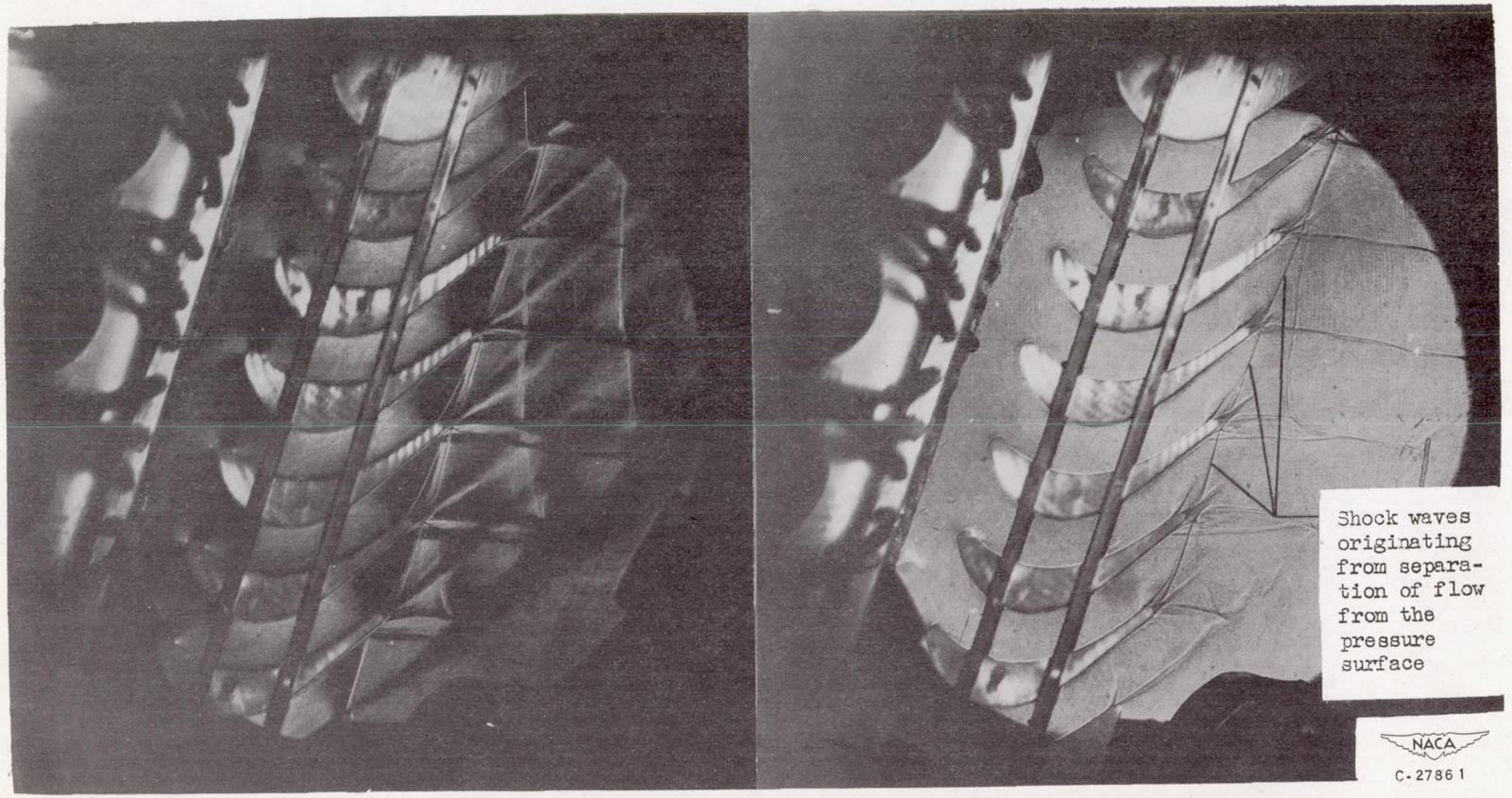

(c) Schlieren photograph; total-to-static pressure ratio, 3.06.

(d) Schlieren photograph; total-to-static pressure ratio, 3.41.

Figure 8. - Continued. Optical studies of configuration I.

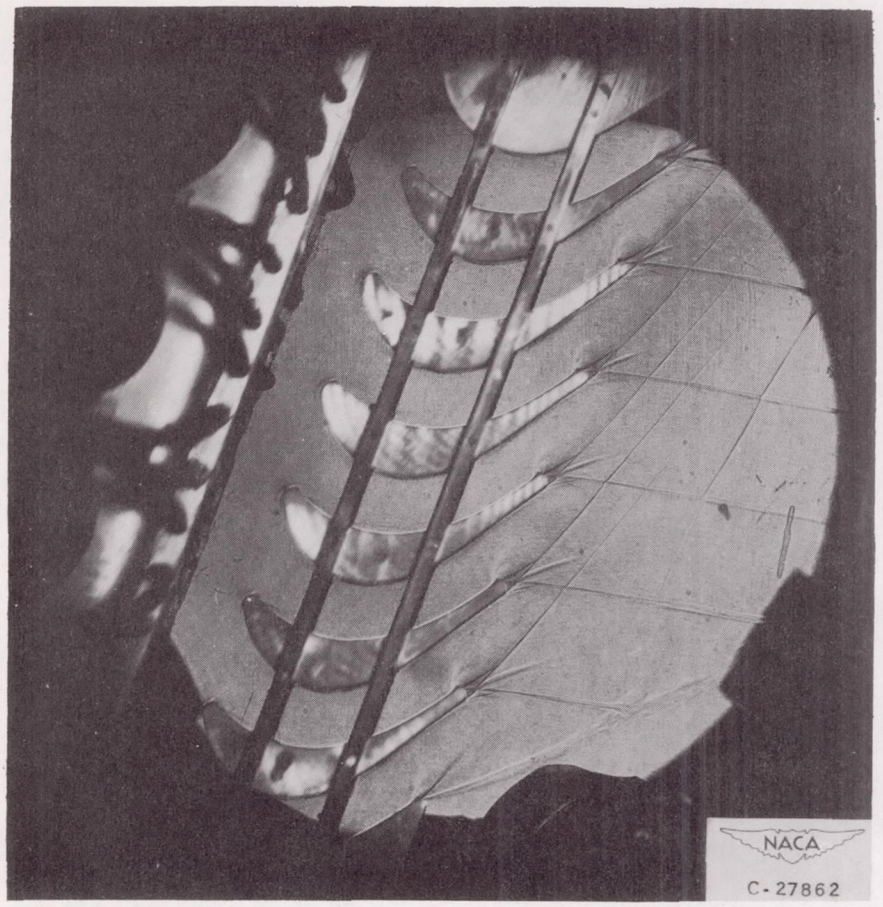

(e) Schlieren photograph; total-to-static pressure ratio, 7.20.

Figure 8. - Concluded.- Optical studies of configuration I.

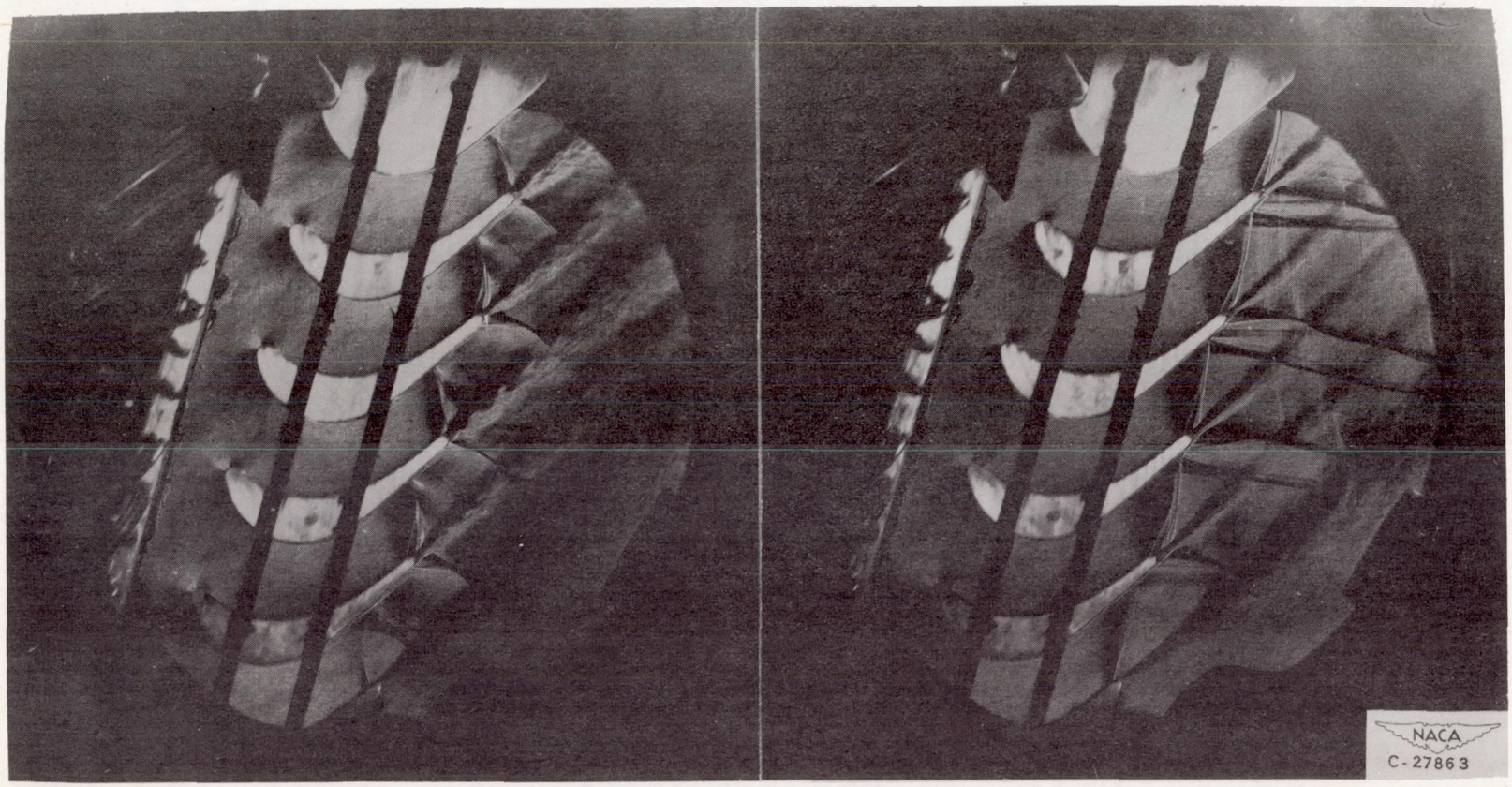

(a) Schlieren photograph; total-to-static pressure ratio, 1.97.

(b) Schlieren photograph; total-to-static pressure ratio, 2.78.

Figure 9. - Optical studies of configuration II.

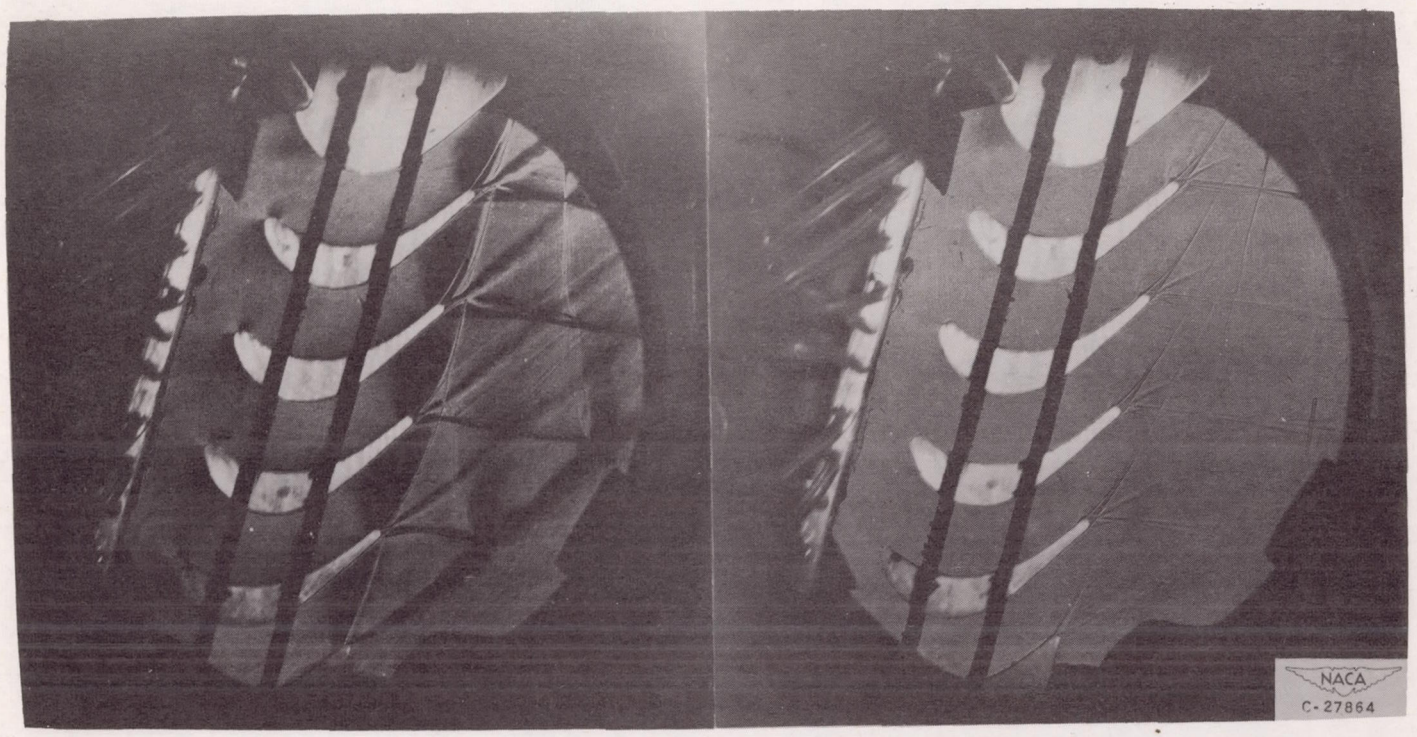

(c) Schlieren photograph; total-to-static pressure ratio, 3.28.

(d) Schlieren photograph; total-to-static pressure ratio, 5.00.

Figure 9. - Concluded. Optical studies of configuration II.

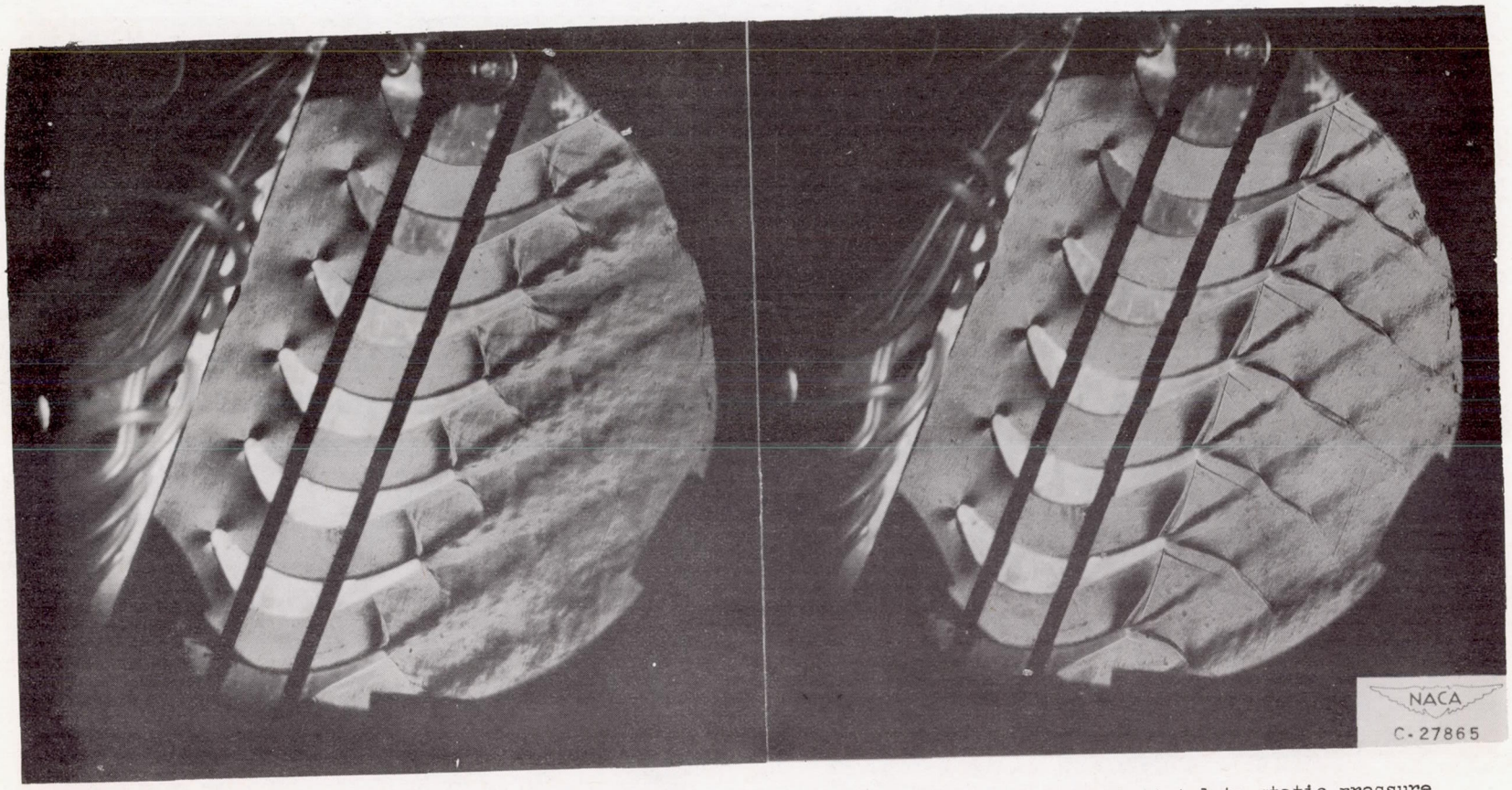

(a) Schlierein photograph; total-to-static pressure ratio, 1.88.

(b) Schlieren photograph; total-to-static pressure ratio, 2.15

Figure 10. - Optical studies of configuration III.

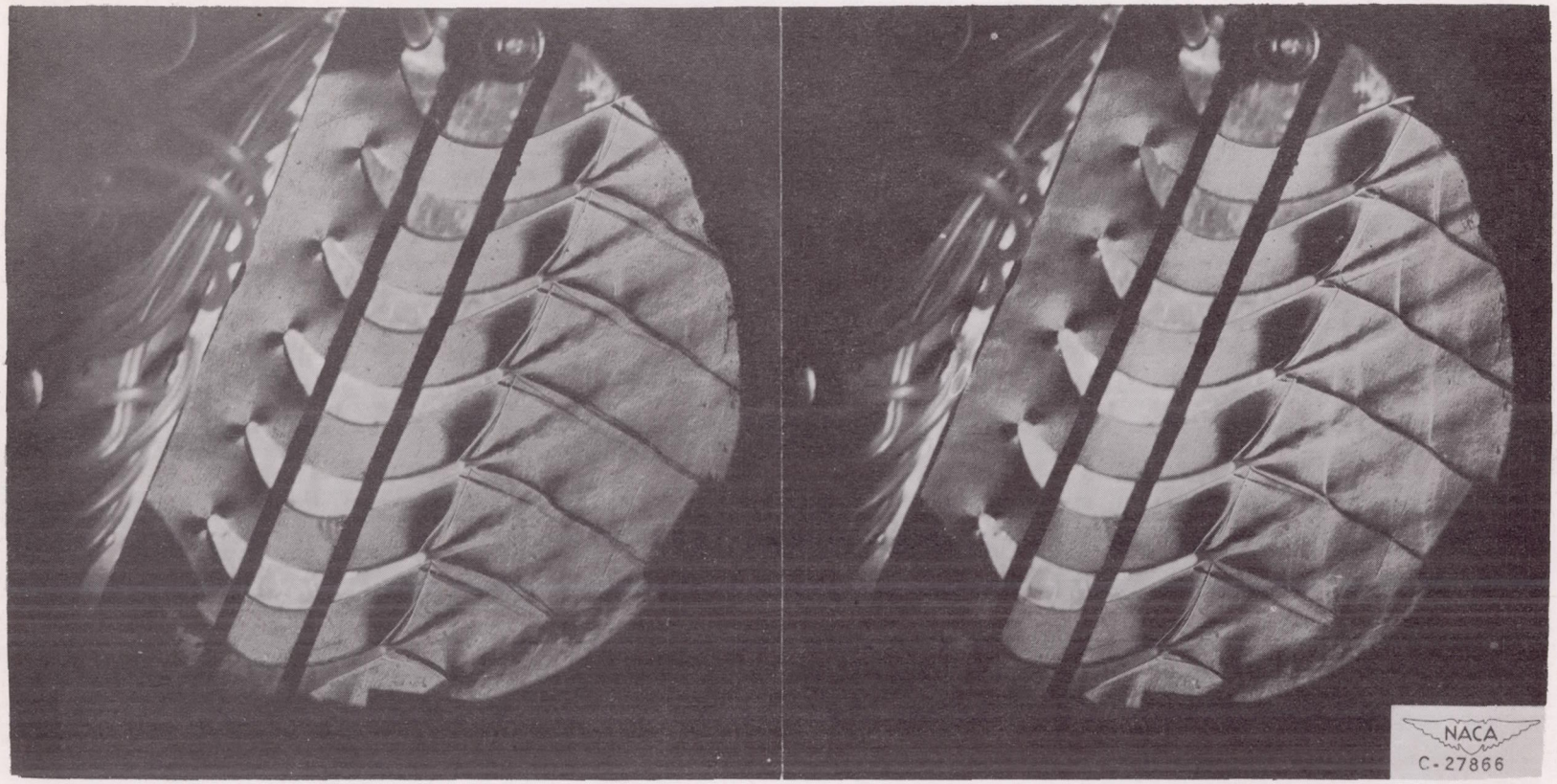

(c) Schlieren photograph; total-to-static pressure ratio, 2.42.

(d) Schlieren photograph; total-to-static pressure ratio, 2.72.

Figure 10. - Continued. Optical studies of configuration III.

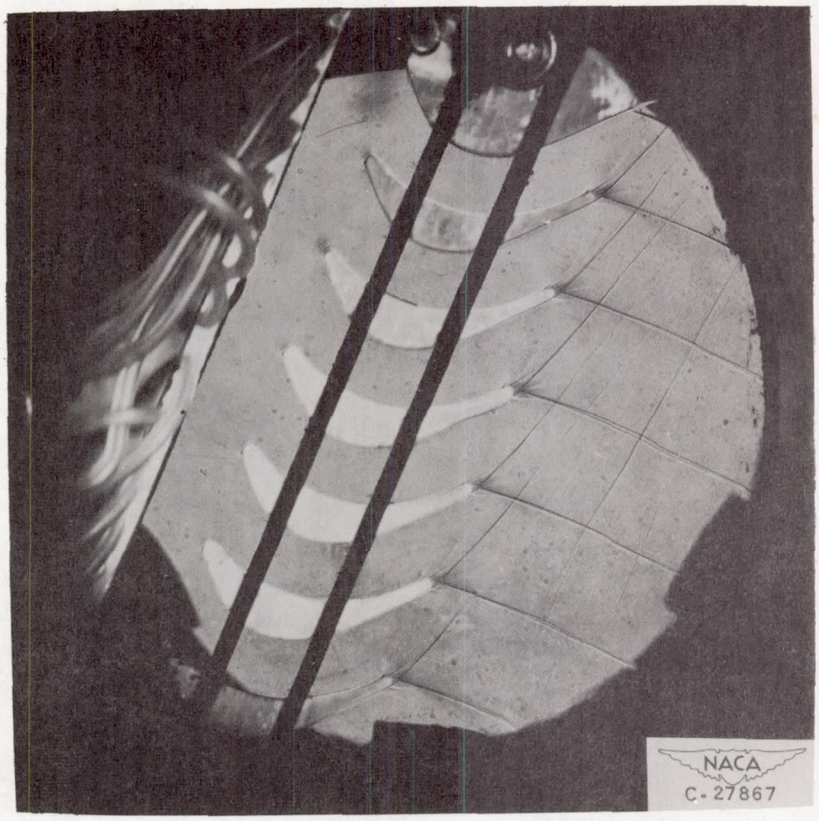

(e) Schlieren photograph; total-to-static pressure ratio, 5.40.

Figure 10. - Concluded. Optical studies of configuration III.

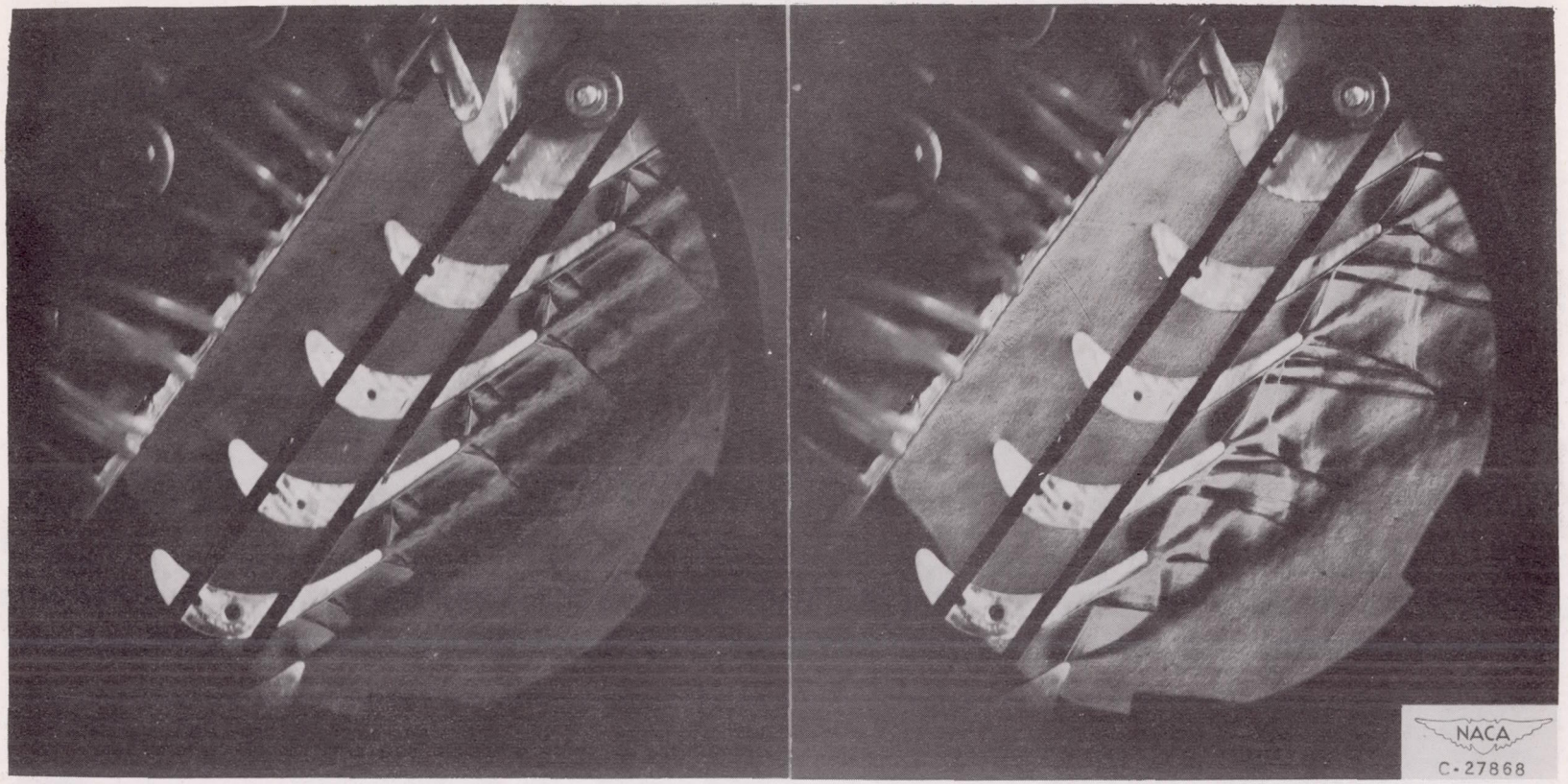

(a) Schlieren photograph; total-to-static pressure ratio, 1.96.

(b) Schlieren photograph; total-to-static pressure ratio, 3.41.

Figure 11. - Optical studies of configuration IV.

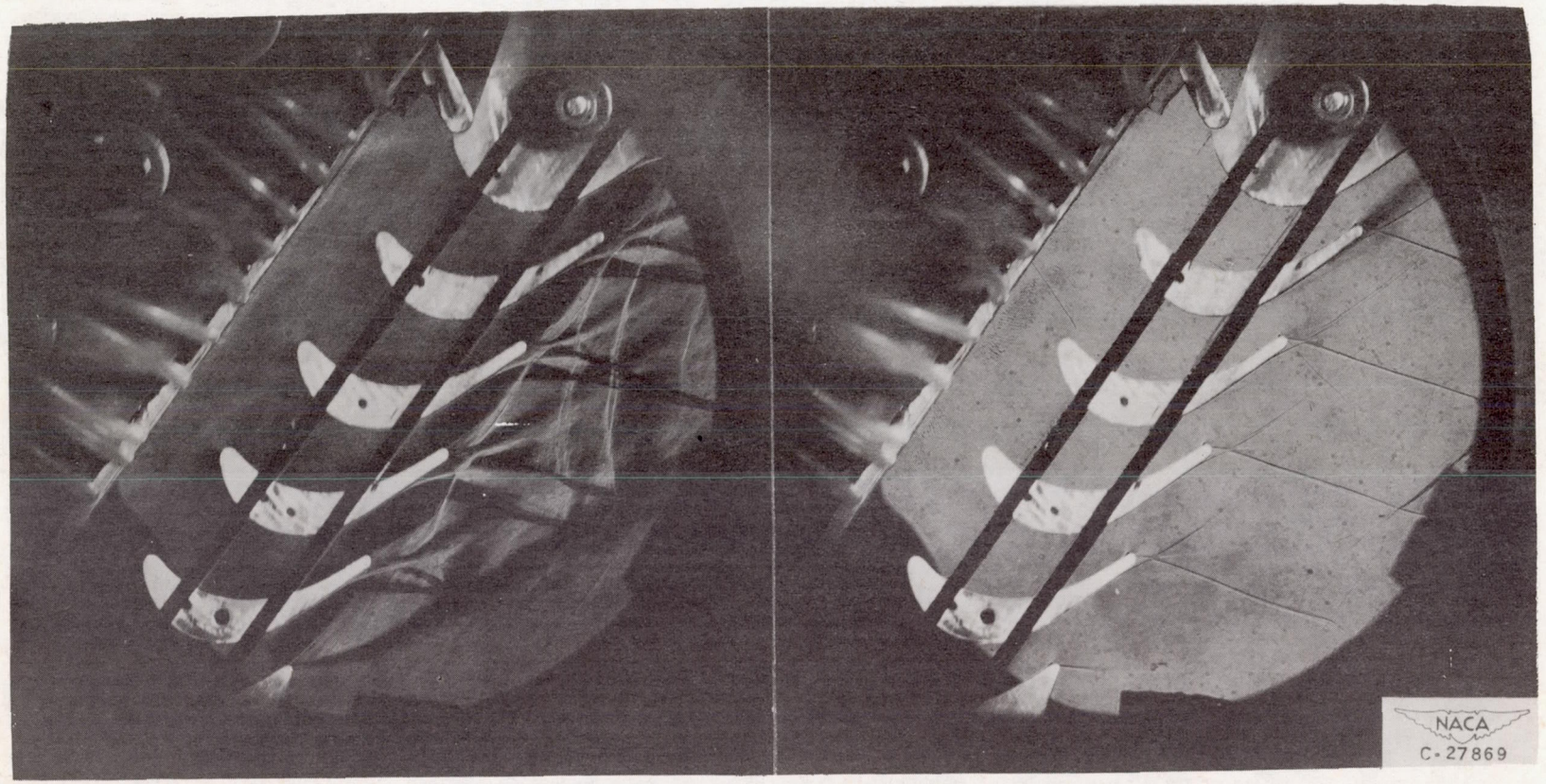

(c) Schlieren photograph; total-to-static pressure ratio, 4.39.

(d) Schlieren photograph; total-to-static pressure ratio, 13 90.

Figure 11. - Concluded. Optical studies of configuration IV.